UPGRADE OF MAD-X FOR HL-LHC PROJECT AND FCC STUDIES

L. Deniau*, A. Latina, T. Persson, I. Shreyber, P. Skowronski,
H. Burkhardt, R. De Maria, M. Giovannozzi, J.M. Jowett, F. Schmidt, CERN, Meyrin, Switzerland
T. Gläßle, HIT, Heidelberg, Germany

Abstract

The design efforts for the High Luminosity upgrade project of the Large Hadron Collider (HL-LHC) and for the FCC-ee studies required significant extensions of the MAD-X code, widely used for designing and simulating particle accelerators. The modelling of synchrotron radiation effects has recently been reviewed, improved, and tested on the lattices of ESRF, LEP, and CLIC Final Focus System. The results were cross checked with several codes, such as AT, PLACET, Geant4, and MAD8. The implementation of space charge has been deeply restructured into a fully modular design. The linear coupling calculation has been completely reviewed and improved to ensure its robustness in the presence of strong coupling effects as is the case for some HL-LHC studies. The slicing module has been generalized to allow for generating thick slices of bending magnets, quadrupoles and solenoids. The SBEND element has been extended to take into account not only the bending angle, but also the integrated dipole strength. Patches have been added to the list of supported elements. Finally, the PTC program inside MAD-X has been extended to provide the tracking of resonance driving terms along lattices, as well as an AC dipole element.

INTRODUCTION

MAD-X is a code to simulate beam dynamics and design beam optics, which was released in 2002. Although it has been tailored to the needs of the LHC, it still remains the most used tool for optics design inside and outside CERN. In order to extend the MAD-X capabilities to better satisfy the users' needs, in particular for the HL-LHC project and the FCC study, several new features have been implemented. An example of such a new feature is the synchrotron radiation, which has a negligible effect on the beam dynamics in the LHC, but plays a major role for the FCC-ee future collider. An element to rotate the coordinate system along the x- and y-direction has also recently been added.

Moreover, to be ready for future studies, several parts of the code and the underlying physics have been reviewed or improved. In this paper we present the clean up of space-charge code as well as of the review of the linear coupling.

An important extension to MAD-X is the Polymorphic Tracking Code (PTC) by E. Forest [1]. In this paper, some of the recently added features, including the possibility to obtain the Resonance Driving Terms (RDT) in the PTC_TWISS table will be presented and discussed.

---

* laurent.deniau@cern.ch

SYNCHROTRON RADIATION EFFECTS

The effects of synchrotron radiation were originally implemented in MAD8 for the needs of the high-energy e^+e^- collider ring LEP at CERN [2]. This implementation was ported to MAD-X and has recently been reviewed and improved. Note that the review of the implementation of synchrotron radiation emission as a quantum phenomenon revealed the presence of a bug in MAD-X versions earlier than 5.04.01. The bug was corrected and the new implementation tested in several cases.

Synchrotron radiation emission is included in the modules TWISS, TRACK, and EMIT at four different levels:

1. No radiation, corresponding to the usual Hamiltonian dynamics.
2. Deterministic radiation, in which all particles radiate the same energy as a single particle on the closed-orbit (TWISS and TRACK). This gives a Hamiltonian system with the correct tunes and closed orbit, including the "stable phase angle" and "energy sawtooth" in electron rings.
3. Deterministic radiation with full dependence on canonical coordinates to generate radiation damping naturally (EMIT, TRACK). Since this method exposes the full dissipative structure of the non-linear phase space dynamics, it is the preferred method for dynamic aperture calculations in high-energy lepton rings [3].
4. Tracking with individual stochastic photon emissions, to provide quantum excitation and particle distributions (TRACK) and equilibrium emittances from first principles. Both the probability of photon emission, i.e. an instantaneous Poisson distribution, and the generation of the random photon-energy distribution depend on the *local* magnetic field and canonical coordinates of the particle.

The MAD-X implementation has been benchmarked against MAD8 using a conversion of the LEP-optics database to the MAD-X format. Rather than attempting to reproduce old results dating from the LEP times, this conversion allowed to run equivalent simulations with MAD8 and MAD-X so that results could be compared in detail. Quantities such as radiation damping rates, equilibrium emittances, energy sawtooth, and the Bassetti component [4] of the horizontal closed orbit $x_c - D_x p_{tc}$, where x_c is the position coordinate of the closed orbit, and p_{tc} is the momentum deviation of the closed orbit, are in excellent agreement between the two codes, confirming that the physics implemented in MAD8 has been preserved in MAD-X.

In addition, MAD-X was tested against other established codes capable of dealing with particle tracking in presence

of synchrotron radiation, such as PLACET [5] and AT [6], providing in all cases an excellent agreement.

Among the test cases considered, the quadrupole doublet of the final focus of CLIC was studied. In these magnets the radiation effects have a significant impact on the beam size and beam shape at the interaction point (IP), through the so-called Oide effect [7]. Figure 1 shows a direct comparison between the phase space of a multi-particle beam, composed of 10^5 macro-particles, at the IP of CLIC assuming a 3 TeV energy in the centre-of-mass, as simulated by the tracking code PLACET and by MAD-X, including stochastic photon emission.
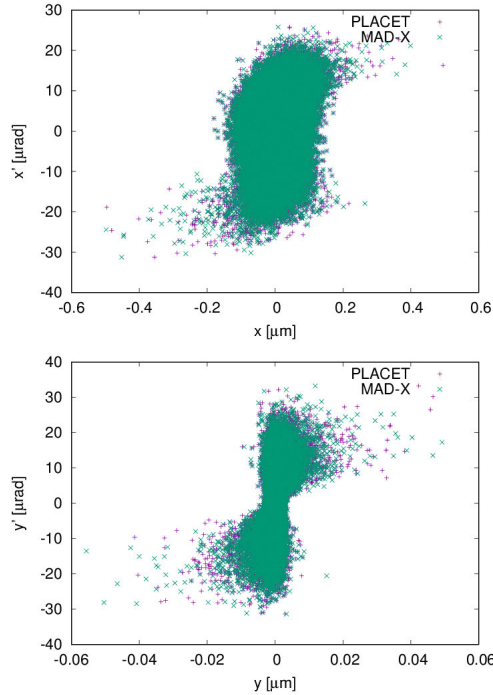
Figure 1: Comparison of phase-space distributions at the IP of CLIC, at 3 TeV centre-of-mass energy, as tracked by PLACET and MAD-X through the final-focus quadrupole doublet, with synchrotron radiation emission simulated as quantum photon emission.

SPACE-CHARGE IMPLEMENTATION

The frozen space-charge model was introduced in MAD-X for the CERN PS injector studies since 2012 [8], and evolved over the past years. The initial implementation was interleaved within the tracking code making efficient support difficult, hence the space-charge implementation has been reviewed and cleaned up. No modifications to the actual physics modelling have been introduced for the time being. However, the code was restructured and made more modular. In the previous implementation the space-charge and beam-beam codes had been interleaved with the code of the modules TWISS and TRACK. A new FORTRAN module was created to gather together all routines related to space-charge

and beam-beam, and a new set of initialization routines have been created to minimize the coupling between the code and other modules like TWISS and TRACK.

The new code has been designed so to facilitate further separation of the space-charge routines from the beam-beam routines, and to open the possibility to create a dedicated MAD-X space-charge command in future. It will also facilitate parallel execution using OPENMP directives.

REVIEW OF LINEAR COUPLING

This section establishes the equations found in the MAD8 physics guide [9] as implemented in MAD-X, and proposes some improvements. A review [10] has been launched after some puzzling results about (nonphysical) negative-value beta functions reported in the framework of HL-LHC studies carried out with strong linear-coupling sources.

The transverse linear coupling calculation for stable motion consists of finding a similarity R_M that transforms a map M describing the motion from s_1 to s_2 into its normal form $M_\perp$.

$$\vec{X}(s_2) = M\vec{X}(s_1),$$

$$M = \begin{pmatrix} A & B \\ C & D \end{pmatrix} = R_M \begin{pmatrix} E & 0 \\ 0 & F \end{pmatrix} R_M^{-1} = R_M M_\perp R_M^{-1}.$$

A linear dynamics is fully described by an s-dependent quadratic Hamiltonian around a reference trajectory

$$\mathcal{H} = \frac{1}{2}\vec{X}^T H \vec{X},$$

where H is a real symmetric matrix that characterizes the equations of motion

$$x_i' = \frac{\partial \mathcal{H}}{\partial p_i} \quad \text{and} \quad p_i' = -\frac{\partial \mathcal{H}}{\partial x_i} \quad \Rightarrow \quad \vec{X}' = SH\vec{X},$$

where S is the fundamental symplectic unit matrix:

$$S = \begin{pmatrix} S_2 & 0 \\ 0 & S_2 \end{pmatrix}, \quad S_2 = \begin{pmatrix} 0 & 1 \\ -1 & 0 \end{pmatrix}, \quad \begin{matrix} S^{-1} = S^T = -S, \\ S^2 = -I. \end{matrix}$$

The map M is the linear solution of these equations of motion and any bilinear Hamiltonian can be brought to the following form by a suitable canonical transformation:

$$\mathcal{H} = \frac{p_x^2 + p_y^2}{2(1 + \delta_P)} + \frac{1}{2}(Fx^2 + Gy^2) + Kxy + L(yp_x - xp_y),$$

where the coefficients F, G, K, L are related to the magnet strengths k_0 (dipole), k_1 (quadrupole) and k_s (solenoid), and the curvature h by [10]:

$$F = hk_0 + k_1 + k_s^2, \quad G = -k_1 + k_s^2,$$
$$K = k_1^s, \qquad\qquad L = k_s.$$

Initialization of coupling calculation

As $M \in \mathrm{Sp}(4, \mathbb{R})$ then

$$\mathrm{eig}(M) = \mathrm{eig}(M^{-1}) = \{(\lambda_i, \lambda_i^{-1}), i = 1..2\},$$

$$\mathrm{eig}(M + \bar{M}) = \{\Lambda_i = \lambda_i + \lambda_i^{-1}, i = 1..2\},$$

where $\bar{M}$ denotes the symplectic conjugate of M. The characteristic polynomial for the coupled motion reads

$$\det(M + \bar{M} - \Lambda I) = \begin{vmatrix} A + \bar{A} - \Lambda I & B + \bar{C} \\ C + \bar{B} & D + \bar{D} - \Lambda I \end{vmatrix}$$

$$= \begin{vmatrix} (\mathrm{tr}\, A - \Lambda)I & \overline{C + \bar{B}} \\ C + \bar{B} & (\mathrm{tr}\, D - \Lambda)I \end{vmatrix} = 0,$$

$$(\mathrm{tr}\, A - \Lambda)(\mathrm{tr}\, D - \Lambda) - |C + \bar{B}| = 0,$$

which can be solved for the eigenmodes [11]

$$\Lambda^2 - (\mathrm{tr}\, A + \mathrm{tr}\, D)\Lambda + \mathrm{tr}\, A \,\mathrm{tr}\, D - |C + \bar{B}| = 0,$$

$$\Delta = (\mathrm{tr}\, A - \mathrm{tr}\, D)^2 + 4|C + \bar{B}|,$$

$$\Lambda_A = \frac{1}{2}(\mathrm{tr}\, A + \mathrm{tr}\, D) + \frac{1}{2}\,\mathrm{sign}(\mathrm{tr}\, A - \mathrm{tr}\, D)\sqrt{\Delta},$$

$$\Lambda_D = \Lambda_A^{-1}\left(\mathrm{tr}\, A \,\mathrm{tr}\, D - |C + \bar{B}|\right),$$
$$\Lambda = \lambda + 1/\lambda \Rightarrow \lambda^2 - \Lambda\lambda + 1 = 0$$

$$\Rightarrow \lambda = \frac{1}{2}\left(\Lambda \pm \sqrt{\Lambda^2 - 4}\right),$$

$$\lambda \in \mathbb{C}\backslash\mathbb{R} \iff \Lambda \in (-2, 2),$$

and where stable linear motion implies

$$|\lambda| = 1 \iff \lambda^{-1} = \lambda^* \iff \lambda = e^{\pm i\mu}, \ \mu \in [0, 2\pi),$$

$$\Lambda_{A,D} = \lambda_{A,D} + 1/\lambda_{A,D} = 2\cos\mu_{A,D},$$

$$(\Lambda_A - \Lambda_D)^2 = 4(\cos\mu_A - \cos\mu_D)^2 = \Delta.$$

For any non-zero eigenvectors $\vec{X}$ and $\vec{Y}$, we have [12]

$$\begin{pmatrix} (\mathrm{tr}\, A - \Lambda_A)I & B + \bar{C} \\ C + \bar{B} & (\mathrm{tr}\, D - \Lambda_A)I \end{pmatrix} \begin{pmatrix} X \\ R_A X \end{pmatrix} = 0,$$

$$\begin{pmatrix} (\mathrm{tr}\, A - \Lambda_D)I & B + \bar{C} \\ C + \bar{B} & (\mathrm{tr}\, D - \Lambda_D)I \end{pmatrix} \begin{pmatrix} R_D Y \\ Y \end{pmatrix} = 0,$$

leading to the solutions (full coupling $R_{A,D} \approx \alpha I$)

$$R_A = \frac{C + \bar{B}}{\Lambda_A - \mathrm{tr}\, D}, \quad R_D = \frac{B + \bar{C}}{\Lambda_D - \mathrm{tr}\, A} = -\bar{R}_A.$$

Noting $R = R_A = -\bar{R}_D$, we find:

$$R = -\left(\frac{1}{2}(\mathrm{tr}\, A - \mathrm{tr}\, D) + \frac{1}{2}\,\mathrm{sign}(\mathrm{tr}\, A - \mathrm{tr}\, D)\sqrt{\Delta}\right)^{-1}(C + \bar{B}).$$

The similarity R_M that block-diagonalizes M into $M_\perp$ can be built from the previous eigenvectors:

$$M_\perp = R_M^{-1} M R_M = g^2 \bar{R}_M M R_M$$

$$= g^2 \begin{pmatrix} I & R_D \\ R_A & I \end{pmatrix} \begin{pmatrix} A & B \\ C & D \end{pmatrix} \begin{pmatrix} I & R_D \\ R_A & I \end{pmatrix}$$

$$= g^2 \begin{pmatrix} I & -\bar{R} \\ R & I \end{pmatrix} \begin{pmatrix} A & B \\ C & D \end{pmatrix} \begin{pmatrix} I & \bar{R} \\ -R & I \end{pmatrix} = \begin{pmatrix} E & 0 \\ 0 & F \end{pmatrix},$$

where g has to be determined such that $R_M^{-1} R_M = g^2 \bar{R}_M R_M = I$. Solving last equation for E and F gives:

$$E = g^2(A - \bar{R}C - (BR - \bar{R}DR))$$

$$= (1 + |R|)^{-1}(A - \bar{R}C)(1 + |R|)$$

$$= A - \bar{R}C = A - BR,$$

$$F = g^2(D + RB + (C\bar{R} + RA\bar{R}))$$

$$= (1 + |R|)^{-1}(D + RB)(1 + |R|)$$

$$= D + RB = D + C\bar{R}.$$

The last form of these equations are mentioned in the MAD8 physics guide and used by MAD-X for initializing the coupling calculation.

The factor g^{-1} represents the strength of the coupling and gR its structure between planes A and D, i.e. the 2×2 Rmat coupling matrix in MAD-X. To determine g, we solve:

$$g^2 \bar{R}_M R_M = g^2 \begin{pmatrix} I + \bar{R}R & 0 \\ 0 & I + R\bar{R} \end{pmatrix} = g^2 (1 + |R|)\, I = I.$$

That is $g = (1 + |R|)^{-\frac{1}{2}} = |R_M|^{-\frac{1}{2}}$, hence gR_M is symplectic and so is $M_\perp$. We can also note that $1 + R\bar{R} > 0 \Rightarrow |C + \bar{B}| > -(\Lambda_{A,D} - \mathrm{tr}\, D, A)^2$. The Edwards–Teng parametrization of the coupling structure gR uses $g = \cos\theta$ and $D = -R\tan\theta$, where θ is the angle of their "symplectic rotation" of planes A and D [13].

From the characteristic polynomial using either $\Lambda_{A,D}$, we can express the coupling strength in terms of the eigenmodes:

$$1 - R_A R_D = 1 - \frac{|C + \bar{B}|}{(\Lambda_A - \mathrm{tr}\, D)(\Lambda_D - \mathrm{tr}\, A)} = \frac{\Lambda_D - \Lambda_A}{\Lambda_D - \mathrm{tr}\, A}$$

$$g = \left(\frac{\Lambda_D - \Lambda_A}{\Lambda_D - \mathrm{tr}\, A}\right)^{-\frac{1}{2}} = \left(\frac{\Lambda_A - \Lambda_D}{\Lambda_A - \mathrm{tr}\, D}\right)^{-\frac{1}{2}}.$$

The Twiss parameters are calculated from E and F by:

$$E = \begin{pmatrix} E_{1,1} & E_{1,2} \\ E_{2,1} & E_{2,2} \end{pmatrix} = \begin{pmatrix} \cos\mu_A + \alpha_A \sin\mu_A & \beta_A \sin\mu_A \\ -\gamma_A \sin\mu_A & \cos\mu_A - \alpha_A \sin\mu_A \end{pmatrix},$$

$$\cos\mu_A = \frac{1}{2}\,\mathrm{tr}\, E,$$

$$\sin\mu_A = \mathrm{sign}(E_{1,2})\sqrt{-E_{1,2}E_{2,1} - \left(\frac{E_{1,1} - E_{2,2}}{2}\right)^2}$$

$$\beta_A = \frac{E_{1,2}}{\sin\mu_A}, \ \gamma_A = -\frac{E_{2,1}}{\sin\mu_A}, \ \alpha_A = \frac{E_{1,1} - E_{2,2}}{2\sin\mu_A},$$

$$M_\perp \in \mathrm{Sp}(4, \mathbb{R}) \Rightarrow \det E = 1 \Rightarrow \beta_A \gamma_A - \alpha_A^2 = 1.$$

The same calculation is performed using F for the second mode.

Propagation of coupling calculation

From the known decoupled map $M_{1\perp}$ at point 1 (from initialization) and the transport map M_{12} from points 1 to 2,

we look after the unknown decoupled map $M_{2\perp}$:

$$M_2 = M_{12}M_1M_{12}^{-1}$$
$$= M_{12}\left(R_{M_1}M_{1\perp}R_{M_1}^{-1}\right)M_{12}^{-1},$$
$$M_{2\perp} = R_{M_2}^{-1}M_2R_{M_2}$$
$$= \left(R_{M_2}^{-1}M_{12}R_{M_1}\right)M_{1\perp}\left(R_{M_1}^{-1}M_{12}^{-1}R_{M_2}\right)$$
$$= W_{12}M_{1\perp}W_{12}^{-1}.$$

Since the eigenmodes 1 and 2 in $M_{1\perp}$ and $M_{2\perp}$ are independent from each other, W_{12} is either block or anti-block diagonal and equality $R_{M_2}W_{12} = M_{12}R_{M_1}$ can take the forms:

$$g_2\begin{pmatrix} I & \bar{R}_2 \\ -R_2 & I \end{pmatrix}\begin{pmatrix} E_{12} & 0 \\ 0 & F_{12} \end{pmatrix} = g_1\begin{pmatrix} A_{12} & B_{12} \\ C_{12} & D_{12} \end{pmatrix}\begin{pmatrix} I & \bar{R}_1 \\ -R_1 & I \end{pmatrix},$$
$$g_2\begin{pmatrix} I & \bar{R}_2 \\ -R_2 & I \end{pmatrix}\begin{pmatrix} 0 & E_{12} \\ F_{12} & 0 \end{pmatrix} = g_1\begin{pmatrix} A_{12} & B_{12} \\ C_{12} & D_{12} \end{pmatrix}\begin{pmatrix} I & \bar{R}_1 \\ -R_1 & I \end{pmatrix}.$$

Solving for E_{12}, F_{12} and R_2 for the block (left) and anti-block (right) diagonal cases gives:

$$\begin{array}{l|l}
E_{12} = g_{12}(A_{12} - B_{12}R_1) & E_{12} = g_{12}(B_{12} + A_{12}\bar{R}_1) \\
F_{12} = g_{12}(D_{12} + C_{12}\bar{R}_1) & F_{12} = g_{12}(C_{12} - D_{12}R_1) \\
R_2 = -g_{12}(C_{12} - D_{12}R_1)E_{12}^{-1} & R_2 = -g_{12}(D_{12} + C_{12}\bar{R}_1)E_{12}^{-1}
\end{array}$$

where $g_{12} = g_1g_2^{-1}$. The sector map $M_{2\perp}$ at point 2 is then calculated by propagating $M_{1\perp}$ through M_{12} using,

$$\begin{array}{l|l}
E_2 = E_{12}E_1\bar{E}_{12}/|E_{12}| & E_2 = E_{12}F_1\bar{E}_{12}/|E_{12}| \\
F_2 = F_{12}F_1\bar{F}_{12}/|F_{12}| & F_2 = F_{12}E_1\bar{F}_{12}/|F_{12}| \\
R_2 = -(C_{12} - D_{12}R_1)\dfrac{\bar{E}_{12}}{|E_{12}|} & R_2 = -(D_{12} + C_{12}\bar{R}_1)\dfrac{\bar{E}_{12}}{|E_{12}|}
\end{array}$$

A flip mode [14] was introduced in MAD-X to solve the problem of negative beta functions that occurred when $|A_{12} - B_{12}R_1| < \varepsilon$ or $|D_{12} + C_{12}\bar{R}_1| < \varepsilon$ for some small positive ε, and switch from block to anti-block diagonal solutions. So far, MAD-X uses a simplified version of these equations, and generates a warning if the number of flips is odd.

The last step consist of the propagation of the Twiss parameters through M_{12} using $T_2 = W_{12}T_1W_{12}^{-1}$ where,

$$T^{(E,F)} = \begin{pmatrix} \beta & -\alpha \\ -\alpha & \gamma \end{pmatrix},$$

and gives for $T_2^{(E)}$ from E_{12} and $T_1^{(E)}$:

$$\alpha_2 = -((E_{2,1}\beta_1 - E_{2,2}\alpha_1)\times$$
$$(E_{1,1}\beta_1 - E_{1,2}\alpha_1) + E_{1,2}E_{2,2})/(|E_{12}|\beta_1)$$
$$\beta_2 = ((E_{1,1}\beta_1 - E_{1,2}\alpha_1)^2 + E_{1,2}^2)/(|E_{12}|\beta_1)$$
$$\mu_2 = \mu_1 + \tan^{-1}(E_{1,2}, (E_{1,1}\beta_1 - E_{1,2}\alpha_1))$$
$$\gamma_2 = (1 + \alpha_2^2)/\beta_2.$$

The same calculation is performed using F for the second mode.

TUPAF01

SLICING MODULE GENERALIZATION

MAD-X contains a slicing module called MAKETHIN. It was originally designed to provide an automatic translation of the thick lattice description to a symplectic thin-lens description, suitable for tracking codes. Previously, both thick and thin lattice description had to be generated and maintained by hand. With MAKETHIN, a single thick-lattice description was sufficient and a thin version was generated automatically when needed for thin-lens tracking. For this, MAKETHIN automatically translates all thick magnets into slices of zero-length multipoles. The number of slices can be chosen using the standard MAD-X selection, i.e. by element class, range or matching patterns in element names. The position of the slices can be chosen as equidistant (MAKETHIN, STYLE=SIMPLE) or using an optimized algorithm (selected by MAKETHIN, STYLE=TEAPOT), which minimizes the beta-beating introduced by using a small number of slices [15].

Slicing turned out to be also very useful for other purposes than thin-lens tracking. The markers generated by MAKETHIN at ends and between slices can be used to obtain the value of optical functions or perform aperture checks within elements. MAKETHIN has gradually become a rather general slicing and automatic lattice editing tool, used also for purposes like aperture or Twiss-parameter interpolation. Elements can be left thick by selecting zero slices, or also by generating thick slices for selected element types. Thick slicing was first implemented for quadrupoles, and then generalized to the slicing of bending magnets [16]. A challenge in thick slicing has been the accurate translation of fringe field effects at the edges of thick elements to the sliced sequences. For bending magnets, this is achieved by generating new thin DIPEDGE elements at the extremities of the original thick dipole, with automatic translation of rectangular dipoles to sector magnets, i.e. RBEND to SBEND.

The improvements and extension of MAKETHIN were implemented aiming at

- providing by default the best algorithms and methods,

- allowing for backward compatibility, if required using switches.

The extensions to MAKETHIN were largely driven by user requests and the need to extend the automatic slicing to new element types and attributes. The most recent extensions, implemented during this year are

- implementation of optional thick slicing of solenoids,

- translation of aperture tolerances,

- writing bending angles to multipoles if different from integrated zero-order multipole strength $k_0\,l$ (see next section).

A more general review of all element and attribute types used in MAD-X has recently been launched with the aim to simplify and unify the MAKETHIN code and to automatically transmit any new element attributes to the sliced sequence.

ELEMENT-SPECIFIC EXTENSIONS

x- and y-rotation

The x- and y-rotations are two recently-implemented features in MAD-X. Both are implemented as new elements and can be inserted at any arbitrary position in a sequence. The purpose is to rotate the reference frame and update the particle's coordinates in the new frame orientation. This is a useful way to reference other elements into a different frame. The full map used by the tracking code for a x-rotation of angle θ is described by the equations:

$$
\begin{aligned}
x^f &= x^i + \frac{y p_x^i \tan\theta}{p_z^i - p_y^i \tan\theta} \\
p_x^f &= p_x^i \\
y^f &= \frac{y^i}{\cos\theta - p_y^i \tan\theta / p_z^i} \\
p_y^f &= p_y^i \cos\theta + p_z^i \sin\theta \\
t^f &= t_i - \frac{y^i (1/\beta_0 + p_t)\tan\theta}{p_z^i - p_y^i \tan\theta},
\end{aligned}
$$

where x, y are the horizontal and vertical positions, p_x, p_y are the transverse momenta, t is the time difference in relation to the reference particle, β_0 is the relativistic factor, $p_t = (E - E_0)/P_0 c$, where E is the energy and P is the momentum, and $p_z = \sqrt{(1+\delta_p)^2 - p_x^2 - p_y^2}$ with $(1+\delta_p)^2 = 1 + 2p_t/\beta_0 + p_t^2$. The index i refers to the initial state before the rotation and the f refers to the final state, i.e. after conversion to the new coordinate system.

It is worth noting that even though a rotation followed by a rotation in the opposite direction will return the system to its original state, the same does not hold if the procedure is done with an element that has a length in between the rotations. This can be understood by considering a particle with $p_x = p_y = 0$ and $p_z > 0$. Applying a rotation around the y-axis, the particle will get a $p_x \neq 0$. If we then let this particle drift in the new reference frame, we will end up in a $x \neq 0$. If we then apply the opposite rotation the $p_x = p_y = 0$ again, but there is still a horizontal non-zero position.

The x- and y-rotation are also implemented in TWISS for first order, where it is implemented by taking the map derivatives expanded and truncated at first order.

SBEND with Angle Different From $k_0 l$

The TRACK and TWISS modules have been extended to support a SBEND element with an angle α different from the integrated strength $k_0 l$. The difference between these two quantities is considered similarly to a field error, i.e. added to user-defined field errors, and treated as such in the thick map of the SBEND or transferred properly to slices, i.e. MULTIPOLE elements, by the MAKETHIN module. For the purpose of the horizontal field curvature h, this difference implies a change of curvature by $\delta h = (\alpha/l - k_0)/(1 + \delta_p)$.

Matching at Arbitrary Positions in Elements

The MATCH command has been extended to support matching constraints at any position inside thick elements [17], and is plan for next MAD-X release. The first step was to implement the interpolation mechanism for the TWISS command. For this purpose, the SELECT command has been extended with the new flag INTERPOLATE and the new attributes AT, SLICE, and STEP to specify the (relative)positions within the selected elements by ranges and patterns. Then, the CONSTRAINT command has been extended with the new IINDEX attribute to specify the index (starting at 0) of the (relative) position in an element where the constraint must hold, as shown in the following command excerpt:

```
SELECT, FLAG=INTERPOLATE, RANGE=mq1, AT={0.5, 1};
MATCH, SEQUENCE=seq;
VARY, NAME=k1; # vary strength of quadrupole mq1
CONSTRAINT, RANGE=mq1, IINDEX=0, BETX=5;
LMDIF;  # match betx at centre of mq1 varying k1
ENDMATCH;
```

MAD-X PTC EXTENSIONS

One of the main methods of measuring non-linear beam parameters is by performing harmonic analysis of the betatronic motion. The beam oscillations are provoked either by a kicker magnet or by an Alternating Current (AC) dipole. The amplitude of the lines present in the spectra are directly linked to strength of the RDTs, whose definition can be found, for instance, in [18] where the detail of the method is also presented.

Modelling RDT propagation along an accelerator structure is a very important topic in computational accelerator physics for several reasons: to compare theoretical predictions with beam-based measurements; to calculate their change upon the action of dedicated corrector magnet in view of constructing response matrices for optimized correction strategies; to test and provide optimization strategies of RDT to achieve an optimal beam performance. In this respect it is worth mentioning that while for some applications the RDTs need to be minimized for others they have to be controlled and different from zero, as is the case for the CERN PS Multi-Turn Extraction (MTE) [19, 20].

RDTs are calculated by PTC_TWISS when the option TRACKRDTS is set to true. The PTC_TWISS algorithm in its core propagates the A^{-1} map along the lattice, as defined by the normal form transformation $M = A^{-1} \cdot R \cdot A$. M is a non-linear map describing the motion along the accelerator. The A^{-1} map transforms the Cartesian coordinates x, p_x, y, p_y to phasors [21], i.e. the normal-form coordinates, $\zeta_{x,+}, \zeta_{x,-}, \zeta_{y,+}, \zeta_{y,-}$, where the Hamiltonian depends only on non-linear amplitudes and is independent of phase advances. Finally, R is an amplitude-dependent rotation.

A^{-1} can be expressed in terms of a generating function F that is a simple polynomial

$$A^{-1} = e^{:-F:} \tag{1}$$

$$F = \sum_{n \geq 2} \sum_{jklm}^{n=j+k+l+m} f_{jklm} \zeta_{x,+}^j \zeta_{x,-}^k \zeta_{y,+}^l \zeta_{y,-}^m, \tag{2}$$

whose coefficients f_{jklm} are the RDTs.

For each lattice element, the calculated coefficients of F are written to a dedicated table called TWISSRDT. The content of this table can be plotted or matched the same way as any other variable present in the TWISS table. Figure 2 shows an example of the comparison of the RDT f_{4000} as computed by PTC_TWISS or from tracking simulations where the excellent agreement is clearly visible. The AC dipole element
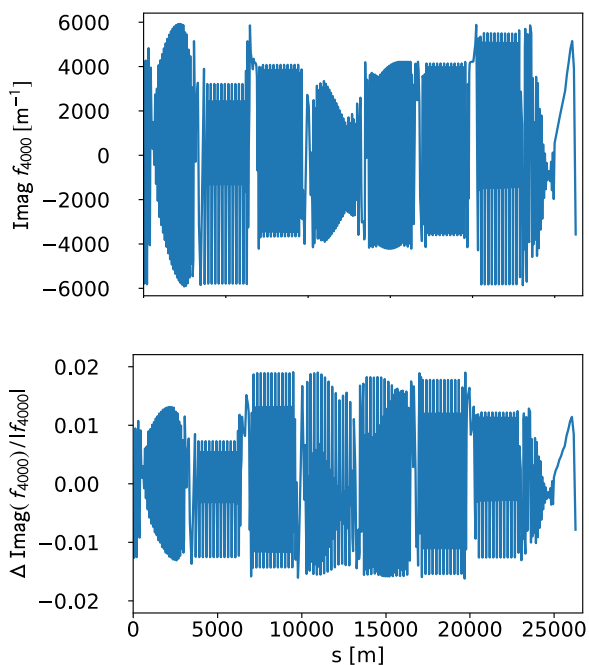
Figure 2: Imaginary part of f_{4000} from PTC_TWISS (upper) and relative difference between RDT- and numerical-tracking simulations for the LHC (lower, courtesy of F. Carlier).

has been interfaced to the PTC_TRACK module so that the dynamics of beams undergoing forced oscillations, as is the case during optics measurements, can now be modelled. It employs a PTC feature called *clock*, which extends the phase space with special variables oscillating proportionally to the beam's time of flight. It can be thought of as an analog hand clock representing rotating vectors (i.e. phasors) with a given frequency. Parameters of the selected magnets can be linked to a clock value at the moment of passage through this magnet, thus yielding oscillatory behaviour on a turn-by-turn basis. Currently, the implementation is limited to two distinct clock frequencies, which is enough to implement the most realistic scenario with one horizontal and one vertical AC dipole. This element also implements ramp up, plateau and ramp down times, as these features are routinely used during optics measurements to excite the beam adiabatically thus avoiding emittance blow up. AC dipoles will be implemented in PTC_TWISS in the near future.

All the PTC options of synchrotron radiation modelling are now interfaced in the MAD-X commands and the possibility to simulate stochastic effects of the radiation were added. Note that PTC_TWISS also outputs damping times and equilibrium emittances.

Several other improvements, bug fixes, and performance optimization have been performed and implemented in the code, and the main ones are:

- Speed up of the sector-bend tracking with the exact Hamiltonian by an automatic detection of the maximum multipole order required in the numerical computations. Indeed, previously it was by default set to 22 to allow for magnetic errors modelling to this level. For the LHC lattice PTC_TWISS computation became three times faster.

- A new option NORMAL of PTC_TWISS writes all the results of the normal form analysis to a dedicated table called NONLIN. Currently, the following variables are provided to the order specified in PTC_TWISS: the three tunes, dispersions, eigenvectors, RDTs (generating function), Hamiltonian, and one-turn map. Note that the same algorithm is available in the PTC_NORMAL command, however, while the non-linear parameters need not to be selected for PTC_TWISS, this is not the case for PTC_NORMAL. It is worth stressing that the format of the output table is such that the parameters can be easily accessed in the subsequent parts of the user script, for example in matching routines.

- RECLOSS option has been implemented in PTC_TRACK that currently produces a table of the last coordinates for each lost particle.

- 6D closed-orbit search when TOTALPATH is true was fixed and now the program correctly calculates the dependence of the beam momentum on RF frequency.

- Last, but not least, the most recent version of the PTC library from E. Forest was included in MAD-X.

CONCLUSION

The latest round of improvements to and development of the MAD-X program fully restores some past functionality of MAD8 in terms of synchrotron radiation effects and extends the capabilities including the possibility of dealing with space-charge effects. This, together with element-specific extensions, the improvements of the linear coupling treatment, and the review of PTC commands, make MAD-X/PTC more flexible, robust, and ready to fulfill the needs of studies of planned and future accelerators.

ACKNOWLEDGEMENTS

REFERENCES

[1] E. Forest, F. Schmidt, and E. Mcintosh, "Introduction to the Polymorphic Tracking Code", Technical Report CERN–SL–2002–044 / KEK 2002-03, `http://cds.cern.ch/record/573082/files/sl-2002-044.pdf`.

[2] F. Barbarin, F.C. Iselin, and J.M. Jowett, "Particle dynamics in LEP at very high-energy", in *Proc. EPAC 1994*, London, England, pp. 193-95, `http://cern.ch/accelconf/e94/pdf/epac1994_0193.pdf`.

[3] J.M. Jowett, "Realistic prediction of dynamic aperture and optics performance for LEP", in *Proc. PAC 1999*, New York, US, pp. 1680–82, TUP86, `http://cern.ch/accelconf/p99/papers/tup86.pdf`.

[4] M. Bassetti, "Effects Due to the Discontinuous Replacement of Radiated Energy in an Electron Storage Ring", *Experientia* **40**, pp. 968, 1980.

[5] D. Schulte *et al.*, "The PLACET Tracking Code", `http://cern.ch/clicsw`.

[6] A. Terebilo, "Accelerator Toolbox for MATLAB", SLAC-PUB-8732, 2001.

[7] K. Oide, "Synchrotron-Radiation Limit on the Focusing of Electron Beams", *Phys. Rev. Lett.* **61**, 1713, 1988.

[8] G. Franchetti, S. Gilardoni, A. Huschauer, F. Schmidt and R. Wasef, "Space charge effects on the third order coupled resonance", *Phys. Rev. Acc. and Beam,* Vol. 20, Iss. 8, 2017.

[9] F. C. Iselin, "The MAD program: Physical Methods Manual", CERN Report SL/92, 1994.

[10] L. Deniau, "MAD-X Linear Coupling Review", CERN BE/ABP-HSS presentations, part 1 & part 2, 2017.

[11] E.D. Courant, and H.S. Snyder, "Theory of the Alternating-Gradient Synchrotron", *Annals of Physics* **3**, pp. 360-408, 1958.

[12] J. Eisenfeld, "Block diagonalization and eigenvalues", *Linear Algebra and its Application* **15**, pp. 205–215, 1976.

[13] D.A. Edwards, and L.C. Teng, "Parametrization of linear coupled motion in periodic systems", *IEEE Trans. on Nuclear Science* **20**, pp. 885–888, 1973.

[14] D. Sagan, and D. Rubin, "Linear analysis of coupled lattices", *Phys. Rev. ST Accel. Beams* **2**, 074001, 1999.

[15] H.Burkhardt *et al.*, "Improved TEAPOT Method and Tracking with Thick Quadrupoles for the LHC and its Upgrade", in *Proc. IPAC 2013*, Shanghai, China, pp. 945–947, MOPWO027, `http://cern.ch/accelconf/IPAC2013/papers/mopwo027.pdf`.

[16] H. Burkhardt, L. Deniau, and A. Latina, "Upgrade of Slicing and Tracking in MAD-X", in *Proc. IPAC 2014*, Dresden, Germany. `doi:10.18429/JACoW-IPAC2014-TUPRO063`

[17] T. Gläßle, "Report on collaboration on MAD-X extensions and GUI for tuning of transfer lines", Technical Report, 2017.

[18] A. Franchi *et al.*, "First simultaneous measurement of sextupolar and octupolar resonance driving terms in a circular accelerator from turn-by-turn beam position monitor data", *Phys. Rev. ST Accel. Beams* **17**, 074001, 2014.

[19] R. Cappi, and M. Giovannozzi, "Novel Method for Multi-Turn Extraction: Trapping Charged Particles in Islands of Phase Space", *Phys. Rev. Lett.* **88**, 104801, 2002.

[20] A. Huschauer *et al.*, "Transverse Beam Splitting Made Operational: Key Features of the Multi-Turn Extraction at the CERN Proton Synchrotron", *Phys. Rev. Accel. Beams* **20**, 061001, 2017.

[21] E. Forest, "From tracking code to analysis: generalised Courant-Snyder theory for any accelerator model", *Springer,* 2016.